Journal of Alloys and Compounds 805 (2019) 852–858

Contents lists available at ScienceDirect

Journal of Alloys and Compounds

journal homepage: http://www.elsevier.com/locate/jalcom

Crystal structure and microwave dielectric properties of a new low-loss ceramic $NiTiTa_2O_8$

Shiyuan Wang, Jundan Chen, Yujuan Zhang, Yingchun Zhang*

University of Science and Technology Beijing, School of Material Science and Engineering, Beijing, 100083, PR China

ARTICLE INFO

Article history:
Received 8 May 2019
Received in revised form
8 July 2019
Accepted 11 July 2019
Available online 12 July 2019

Keywords:
$NiTiTa_2O_8$
Dielectric properties
Ceramics
Low-loss
Tantalates

ABSTRACT

A new microwave dielectric ceramic $NiTiTa_2O_8$ with tetragonal cell of the trirutile-type structure was reported in this study. The crystal structure, microstructure, sintering behavior, and microwave dielectric properties of $NiTiTa_2O_8$ ceramics were investigated. Crystallographic parameters were acquired by Rietveld refinement and lattice potential energy, theoretical dielectric constant, packing fraction as well as distortions of the octahedron were calculated. $NiTiTa_2O_8$ ceramics sintered at 1350 °C possessed the most stable structure with refined parameters being $a = b = 4.6869(2)$ Å, $c = 9.0726(1)$ Å and $V_{unit} = 199.617$ Å^3. The measured dielectric constants, all sensitive to the density of samples, were lower than those of theoretical values. The $Q \times f$ values were largely linked to the packing fraction and relative density. The temperature coefficient of resonance frequency (τ_f) were mainly influenced by the oxygen distortions of the octahedron. Excellent dielectric properties of $\varepsilon_r = 39.86$, $Q \times f = 25{,}051$ GHz and $\tau_f = 75$ ppm/°C for $NiTiTa_2O_8$ ceramics could be obtained as sintering temperature was 1350 °C.

1. Introduction

With the rapid development of mobile phone and wireless communication market, microwave dielectric materials which widely used in microwave components such as filters, resonators, wave guides, duplexer and antennas need to meet more higher requirements. Developing new medium dielectric constant (ε_r) materials with high quality factor (Q) has become more imperative than ever [1]. In 1994, A. Baumgarte et al. first reported the crystal structure of $M^{2+}M^{4+}Nb_2O_8$(M^{2+} = Be, Mg, Ca, Mn, Co, Ni, Zn, Cd; M^{4+} = Ti, Zr, Ge, Sn) system [2]. In 2000, Kim et al. discovered that $ZnTiNb_2O_8$ ceramic possessed a quality factor of 42,500 GHz, ε_r of 34.3, and τ_f of −52 ppm/°C [3]. Due to the modern communication technology in highly demand, the microwave dielectric ceramics like $CoTiNb_2O_8$, $Cu_{0.5}Ti_{0.5}NbO_4$, $MgTiNb_2O_8$ and $NiTiNb_2O_8$, all belong to niobate-based microwave dielectric ceramics, showing excellent dielectric properties have been studied consecutively [4–9]. However, there were few reports on titanium tantalate-based microwave ceramics. Generally speaking, niobium and tantalum belong to the same family of elements, the ionic radii of Ta^{5+}(0.64 Å) is the same as that of Nb^{5+}(0.64 Å) [10]. Therefore, in order to improve the dielectric properties, many researches focused on the substitution of Nb^{5+} with Ta^{5+} in microwave dielectric ceramics. For example, Mi Xiao et al. found that the $Q \times f$ values and τ_f values were much better as the substitution amount of Ta^{5+} for Nb^{5+} was within a certain range in La $(Nb_{1-x}Ta_x)$ O_4 microwave ceramics [11]. For the $Ni_{0.5}Ti_{0.5}Nb_{1-x}Ta_xO_4$ ceramics reported by Xin Huang et al., the substitution of Nb with Ta changed the bond length, which led to the reduction of the δ Nb—O of the [NbO_6] octahedral and the lowering of τ_f values [12]. And Qingwei Liao et al. reported that the low-temperature sinterable ceramics $ZnTiNbTaO_8$ with relatively excellent properties of ε_r ~36.3, $Q \times f$ ~67,000 GHz, $\tau_f \sim -57.66$ ppm/°C could be obtained by substituting Ta^{5+} for Nb^{5+} [13]. In view of the excellent dielectric properties of $ATiNb_2O_8$ (A = Zn, Mg, Ni, Co et al.) compounds, the possibility of preparing $ATiTa_2O_8$ ceramic have aroused our interest. The study by Jeong-Hyun Park et al. on the crystal structural and microwave dielectric properties of a single phase of $ZnTiTa_2O_8$ ceramic had a positive effect on enriching the research of ATi(Nb, Ta)$_2O_8$ microwave dielectric ceramics [14]. Recently, the new $NiTiTa_2O_8$ materials and $Co_{0.5}Ti_{0.5}TaO_4$ materials were reported by Nobuhiro Kumada et al. *and* Hongyu Yang et al. respectively [15,16]. However, the microwave dielectric properties of $NiTiTa_2O_8$ ceramics, which need to be studied, have not been reported yet. Therefore, in this work, $NiTiTa_2O_8$ ceramics were synthesized via solid reaction. The aim of the paper was to clarify the correlations between crystal

* Corresponding author.
E-mail address: zycustb@163.com (Y. Zhang).

https://doi.org/10.1016/j.jallcom.2019.07.118
0925-8388/

structure, sintering temperature, microstructure and microwave dielectric properties of $NiTiTa_2O_8$ ceramics.

2. Experimental procedures

High-purity NiO (99.9), TiO_2 (99.99), Ta_2O_5 (99.99) powders were used as raw materials. The mixed powder prepared according to the molar ratio was ball milled for 4 h using alcohol as milling medium, then quickly dried and sieved. After calcined at 1250 °C for 2 h, the powder was ball-milled, dried and sieved again, then pressed with 5 wt% polyvinyl alcohol (PVA) into pellets with the pressure of 220 MPa. The pellets were sintered at 1250 °C–1450 °C for 4 h.

The crystal structure of ceramics was identified by X-ray diffraction (XRD, Rigaku, DMAX-RB, Japan) with Cu Kα radiation. The electron diffraction pattern of $NiTiTa_2O_8$ powder was obtained by a transmission electron microscopy (TEM, JEM-2010, JEOL, Japan). The crystallographic parameters were obtained from the Rietveld refinement results of the XRD data using GSAS-EXPGUI software [17,18]. The microstructure of the ceramics was observed by a scanning electron microscopy (SEM, JSM-6710F, JEOL, Japan). The density of the ceramics was confirmed by Archimedes methods. Microwave dielectric properties of the ceramics were measured by a network analyzer (8720 ES, Agilent, USA) using Hakki-Coleman's dielectric resonator method, modified and improved by Courtney and Kobayashi et al. [19–21]. All measurements were conducted in the frequency of 6–9 GHz at room temperature. The temperature coefficients of the resonance frequency (τ_f) were measured in the temperature ranging from 20 to 80 °C. The τ_f values were calculated using the following formula:

$$\tau f = (f_2 - f_1)/f_1(T_2 - T_1)$$

where f 1 and f 2 are the resonance frequency at T_1 and T_2.

3. Results and discussion

3.1. Phase and crystal structure

Fig. 1 presents XRD patterns of $NiTiTa_2O_8$ ceramics sintered at 1250 °C–1450 °C. All diffraction peaks could be indexed with the tetragonal cell of the triutile-type structure (JCPDS: #32–0702, the space group, P42/m n m (#136)) and no other second phase diffraction peaks appeared, suggesting that the $NiTiTa_2O_8$ ceramics remained a stable single phase with trirutile-type structure at different sintering temperature. Furthermore, TEM micrograph and electron diffraction patterns of $NiTiTa_2O_8$ powders calcined at 1250 °C, as shown in Fig. 2, also illustrated that there was only one set of diffraction spots belonging to single-phase structure. By indexing the electron diffraction patterns, it was found that the electron diffraction pattern conformed to the trirutile-type structure. The distance of (110) and (002) lattice planes belonging to [−202] zone axis measured 3.372 Å and 4.503 Å respectively. Above all, the $NiTiTa_2O_8$ compound adopted single phase of the trirutile-type structure through XRD and TEM analysis.

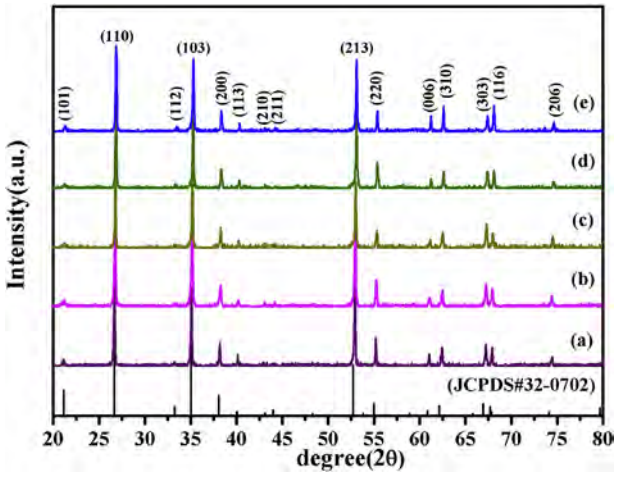

Fig. 1. The XRD patterns of $NiTiTa_2O_8$ ceramics sintered at (a) 1250 °C, (b) 1300 °C, (c) 1350 °C, (d) 1400 °C, (e) 1450 °C.

In order to study more details on the structure of $NiTiTa_2O_8$ ceramics, Rietveld refinement of $NiTiTa_2O_8$ ceramics sintered at 1350 °C was carried out by GSAS-EXPGUI and the XRD profile of the sample after fitting is shown in Fig. 3. The reliability factors R_{wp}, R_p and χ^2 were 9.84, 7.36 and 1.34 respectively, which demonstrated that the structural model was valid and the refinement results were reliable. The calculated lattice parameters were a = b = 4.6869(2) Å, c = 9.0726(1) Å and V_{unit} = 199.617 Å^3. Based on the results of refinement, the structural diagram of $NiTiTa_2O_8$ ceramic is presented in Fig. 4 and Fig. 5. In the trirutile-type $NiTiTa_2O_8$, A-site ions ($Ni_{3/4}Ta_{1/4}$) and B-site ions ($Ti_{3/8}Ta_{5/8}$) were located at *2a* and *4e* Wyckoff positions, while O ions occupied two different positions. The *4f* site was distributed by O_1 and O_2 were in the *8j* Wyckoff position. According to the schematic diagram of the unit cell structure shown in Fig. 4, O_1 and O_2 were both connected with one A-site ion and two B-site ions. The coordination number of all cations was 6. A-site ions and B-site ions were connected with two O_1 and four O_2 to form [AO_6] and [BO_6] octahedrons respectively. Fig. 5 shows the schematic diagram of 3 × 3 × 3 supercell of $NiTiTa_2O_8$. It could be seen that [AO_6] and [BO_6] oxygen octahedrons formed a layered structure in the ratio of 1:2 and extended in the form of … A B B A B B A … along the *c*-axis, with cations arranged in an orderly manner. In the direction of *a*-axis and *b*-axis, [AO_6] and [BO_6] oxygen octahedrons formed zigzag chains by sharing common-edged (such as O_1–O_1). On the plane paralleling to the *ab*-plane, [AO_6] were connected with [AO_6] (or [BO_6]) by sharing common-vertices (such as O_1). In addition, atomic fractional coordinates of the $NiTiTa_2O_8$ ceramics sintered at 1350 °C after refinement are given in Table 1.

3.2. Lattice potential energy

With sintering temperature increasing, the bond length between the atoms in $NiTiTa_2O_8$ ceramics was elongated or compressed inevitably, leading to the structural changes eventually. Herein, the structural evolution of $NiTiTa_2O_8$ ceramics sintered at different temperature was analyzed by Rietveld refinement. Table 2 lists the crystallographic data obtained from Rietveld refinement of $NiTiTa_2O_8$ ceramics sintered at different temperature. From the results, it was found that the unit cell volume first shrunk slightly to 199.300 Å^3 and then expanded to 200.096 Å^3 at the temperature ranging from 1250 °C to 1450 °C. The volume of unit cell first decreased might due to the occurrence of oxygen vacancies in most oxides, which was a common defect that caused lattice distortion. Afterwards, with the continuous rise of temperature, the lattice expansion led to the increase of cell volume. To further study the stability of ceramic structure at different sintering temperatures, lattice potential energy (U_{POT}), a dominant term in the thermodynamic analysis, was calculated by following formulas [22]:

$$U_{POT} = AI(2I/V_m)^{1/3}$$

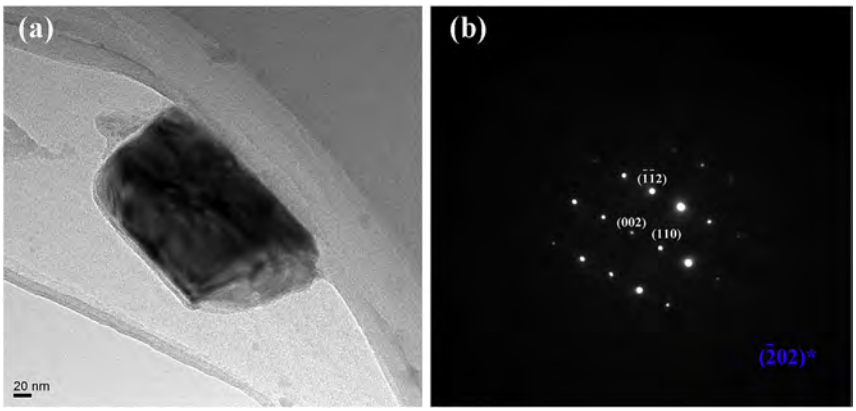

Fig. 2. (a) TEM micrograph and (b) electron diffraction patterns of $NiTiTa_2O_8$ powders calcined at 1250 °C.

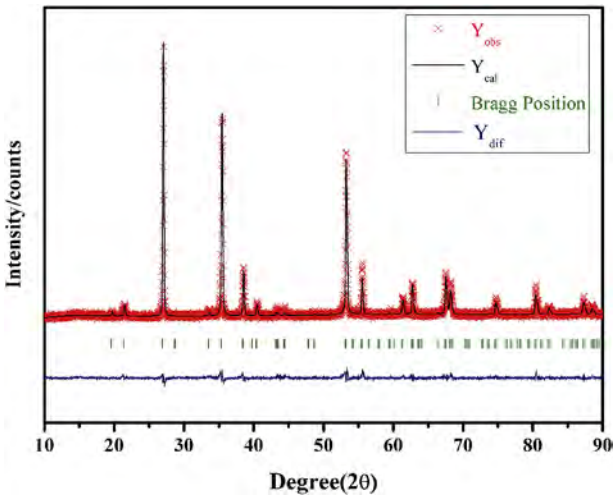

Fig. 3. The Rietveld refinement plot of $NiTiTa_2O_8$ ceramic sintered at 1350 °C.

$$2I = \sum_i n_i Z_i^2$$

where A was a constant value (A = 121.4 kJ mol $^{-1}$ nm), n_i was the number of ions with integer charge Z_i, I was the ionic strength and V_m was the volume per formula units. Fig. 6 illustrates the variation trend of lattice potential energy for $NiTiTa_2O_8$ ceramics sintered at 1250°C-1450 °C. Compared with the unit cell volume in Table 2, the lattice potential energy showed an opposite trend and reached the maximum value (56691.36 kJ/mol) at 1350 °C, which was concluded that $NiTiTa_2O_8$ ceramics sintered at 1350 °C possessed the most stable structure.

3.3. Microstructure and sintering behavior

Fig. 7 shows the SEM images of $NiTiTa_2O_8$ ceramics sintered at different temperature. At 1250 °C, as shown in Fig. 7 (a), there were many pores in the intersection of grains and the grain size was small. In Fig. 7 (c), as the sintering temperature reached 1350 °C, it was evident that the samples exhibited a completely dense microstructure, the average grain size ranged from 9 to 13 μm and the overall microstructure depicted irregular polygonal grains. When the sintering temperature continued to rise, the average

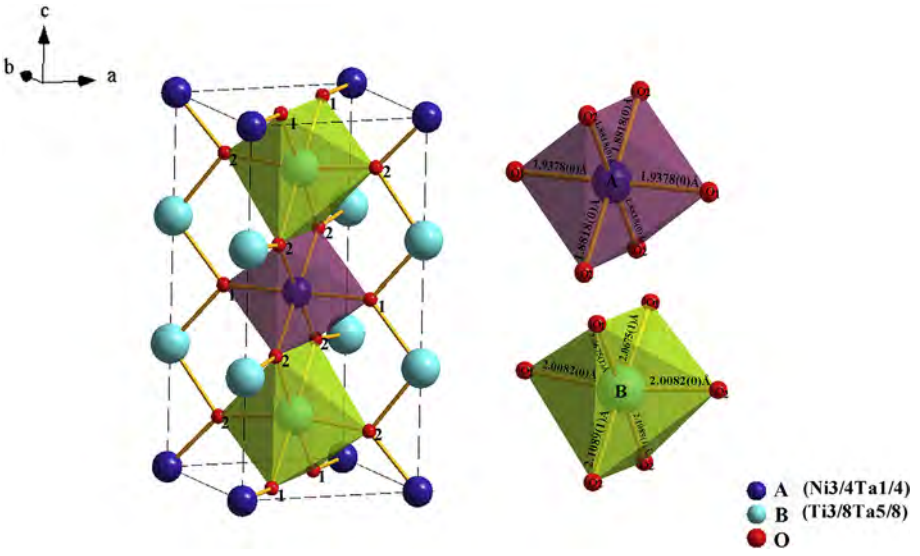

Fig. 4. The schematic diagram of the unit cell structure of $NiTiTa_2O_8$ ceramics sintered at 1350 °C.

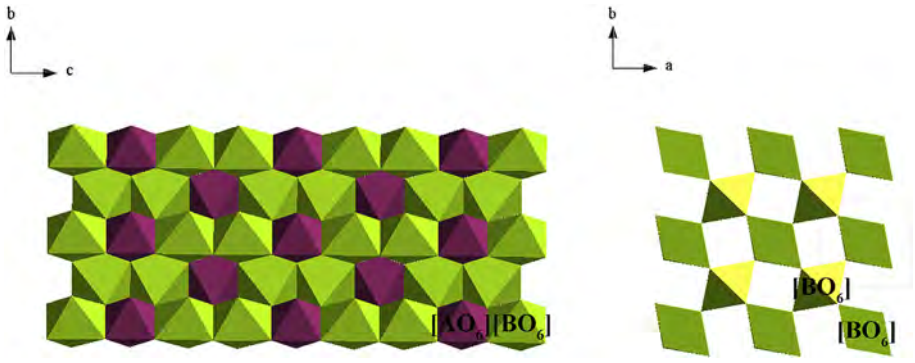

Fig. 5. The schematic diagram of 3 × 3 × 3 supercell structure of $NiTiTa_2O_8$ ceramics sintered at 1350 °C.

Table 1
Atomic fractional coordinates of the $NiTiTa_2O_8$ ceramics sintered at 1350 °C.

atom	position	x	y	z	occupancy	Uiso
Ni	2a	0.00000	0.00000	0.00000	0.750	0.01504
Ta	2a	0.00000	0.00000	0.00000	0.250	0.01504
Ti	4e	0.00000	0.00000	0.32994	0.625	0.00546
Ta	4e	0.00000	0.00000	0.32994	0.375	0.00546
O1	4f	0.29234	0.29234	0.00000	1.000	0.01212
O2	8j	0.30149	0.30149	0.36171	1.000	0.03407

Table 2
Crystallographic data obtained from Rietveld refinement for $NiTiTa_2O_8$ ceramics sintered at different temperature.

St (°C)	lattice Parameters (Å)			V_{unit} (Å^3)	Reliability factors		
	a = b (Å)	c (Å)	α = β = γ		R_{wp} (%)	R_p (%)	χ^2
1250	4.6888(4)	9.0795(9)	90	199.617	8.43	4.38	1.43
1300	4.6879(3)	9.0779(7)	90	199.505	9.26	6.07	1.37
1350	4.6869(2)	9.0726(1)	90	199.300	9.84	7.32	1.36
1400	4.6902(3)	9.0772(9)	90	199.685	9.67	7.66	1.34
1450	4.6926(0)	9.0867(9)	90	200.096	9.42	6.83	1.39

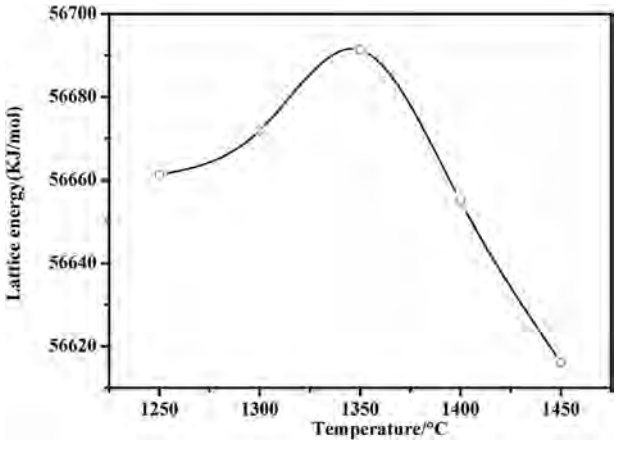

Fig. 6. Lattice potential energy of $NiTiTa_2O_8$ ceramics sintered at different temperature.

grain size increased continuously which was about 20 μm in Fig. 7 (d) and 7 (e), probably an indication of overheating. In addition, it was apparent that, as shown in Fig. 7 (f), a large number of closed stomata of size 1–2 μm existed inside the grains, which could interfere with the microwave dielectric properties of the samples.

Fig. 8 exhibits the curve of the buck density of $NiTiTa_2O_8$ ceramics sintered at different temperatures. As the sintering temperature increased from 1250 °C to 1450 °C, the curve showed that the density of the ceramics increased first which was attributed to the elimination of pores in the intersection of grains, then decreased mainly because of the closed stomata inside the grains and abnormal grain growth shown in Fig. 7. The relative density of samples reached the highest value 94.10% of the theoretical density at 1350 °C. It was worth noting that the optimum sintering temperature of $NiTiTa_2O_8$ ceramics (1350 °C) was higher than that of $NiTiNb_2O_8$ ceramics (1100 °C) [8]. Generally, most of tantalate ceramics had higher sintering temperature than niobate ceramics [23], which could be attributed to the stronger bond energy of Ta–O bond (839 kJ/mol) than Nb–O bond (784 kJ/mol) [24]. There was a firmer binding between ions owing to the stronger bond energy, which made the diffusion of ions more difficult, thus, a higher sintering temperature was required for phase formation.

3.4. Microwave dielectric properties

The dielectric constants of $NiTiTa_2O_8$ Ceramics as a function of sintering temperature are depicted in Fig. 9. The variation trend was consistent with that of density curve in Fig. 8. In general, density was an important factor that affected the dielectric constant of single-phase microwave ceramics [25]. In dense ceramic samples, there were more dipoles per unit volume, which indicated that the ceramic samples were easy to polarize, therefore, the samples exhibited a high dielectric constant [4]. In the case of $NiTiTa_2O_8$ system, the theoretical dielectric constant of ceramics could be obtained by the Clausius-Mossotti equation shown as follows [26,27]:

$$\varepsilon_{cal} = (3V_m + 8\pi\alpha_D)/(3V_m - 4\pi\alpha_D)$$

where α_D was the total polarizability of the substance in molar volume *Vm*. Molecular polarizability of a complex could be calculated by the oxide addition rule [28]:

$$\alpha_D(NiTiTa_2O_8) = \alpha\left(Ni^{2+}\right) + \alpha\left(Ti^{4+}\right) + 2\alpha\left(Ta^{5+}\right) + 8\alpha\left(O^{2-}\right)$$

As shown in Fig. 9, the variation of calculated dielectric constant was in agreement with that of measured value. The calculated dielectric constant of $NiTiNb_2O_8$ ceramics at 1350 °C was close to the measured value (39.86). The slightly distinction between the two values could be attributed to two aspects. On the one hand, the vibration and compression of cations as well as the influence of ionic conductivity and electronic conductivity effected the measured values [29]. On the other hand, density was not taking into account during the theoretical calculation process and the measured values were obtained as the ceramics were not

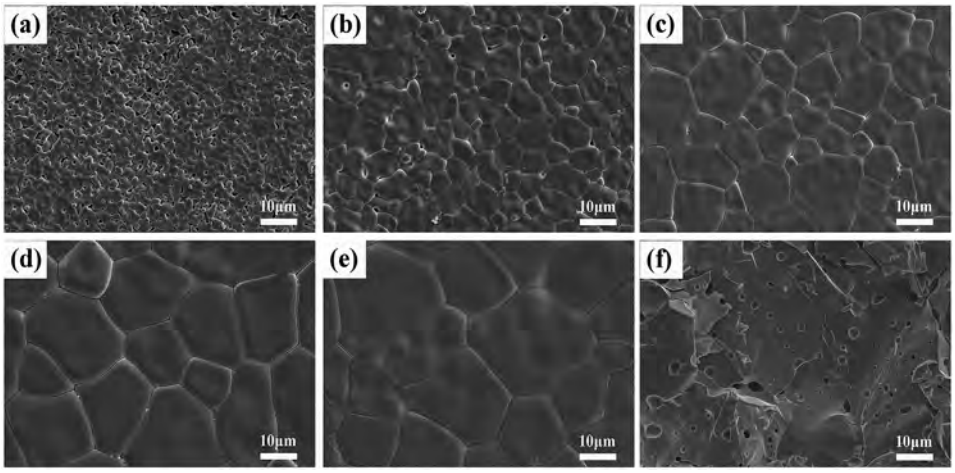

Fig. 7. SEM images of $NiTiNb_2O_8$ ceramics sintered at (a) 1250 °C, (b) 1300 °C, (c) 1350 °C, (d) 1400 °C, (e) 1450 °C and (f) 1400 °C (fracture surface) for 4 h.

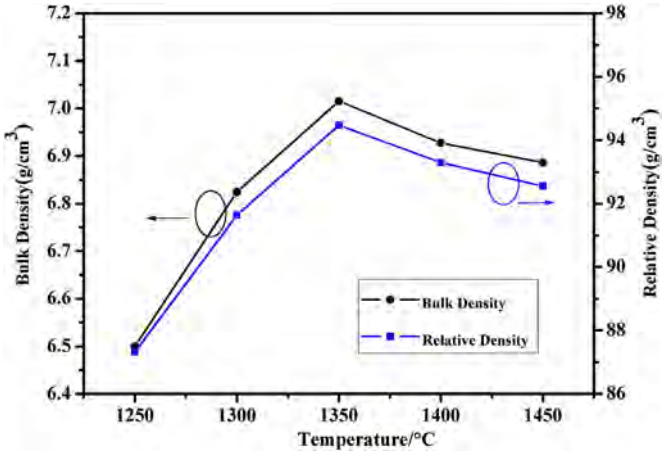

Fig. 8. Buck density and relative density of $NiTiTa_2O_8$ ceramics sintered at different temperatures.

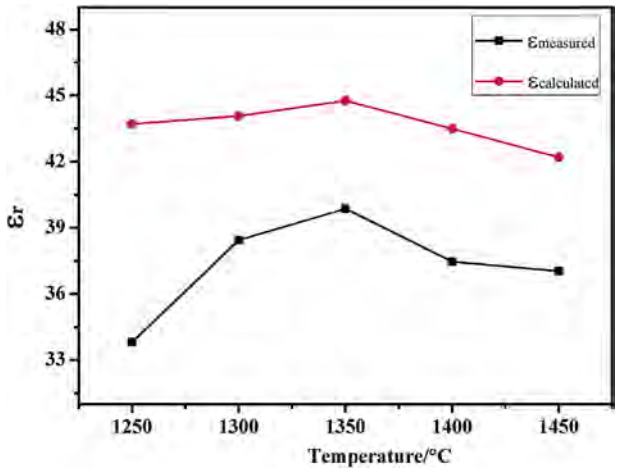

Fig. 9. Variations in the dielectric constants of $NiTiTa_2O_8$ Ceramics as a function of sintering temperature.

completely compact (relative density 94.10%). The air in the pores which had very small dielectric constant ($\varepsilon_r = 1$) would reduce the dielectric constant of the ceramic samples directly. In this work, although the dielectric constant of $NiTiTa_2O_8$ (39.86) was a little smaller than that of $NiTiNb_2O_8$ ceramics (56.8), it was sufficient to meet the requirements of medium dielectric constant materials [8].

Fig. 10 displays the $Q \times f$ values of $NiTiTa_2O_8$ ceramics. The variation of $Q \times f$ values was similar to that of density as shown in Fig. 8. The dielectric loss was largely linked to the crystal structure, lattice defects, density of ceramics, grain size, abnormal growth of crystal grains and excessive oxygen vacancy concentration affected by higher sintering temperature [4]. In this work, the relative density presented a sharp upward at sintering temperature ranging from 1250 °C to 1350 °C. That is to say, the relative density contributed greatly to the dielectric constant within this sintering temperature range. When the temperature was higher than 1350 °C, the $Q \times f$ value mainly was affected by the crystal structure. It was reported that the dielectric loss in the range of microwave frequency was related to the packing fraction of the structure [30]. Packing fraction of $NiTiTa_2O_8$ ceramics could be acquired by the equation as follows:

$$\text{Packing fraction}\ (\%) = \text{Volume of the atoms in the cel}/\text{Volume of primitive unit cell}$$

The decline of packing fraction observed in Fig. 10 led to the increase of lattice vibration and non-harmonic vibration, thus resulting in the decrease of $Q \times f$ values at sintering temperature

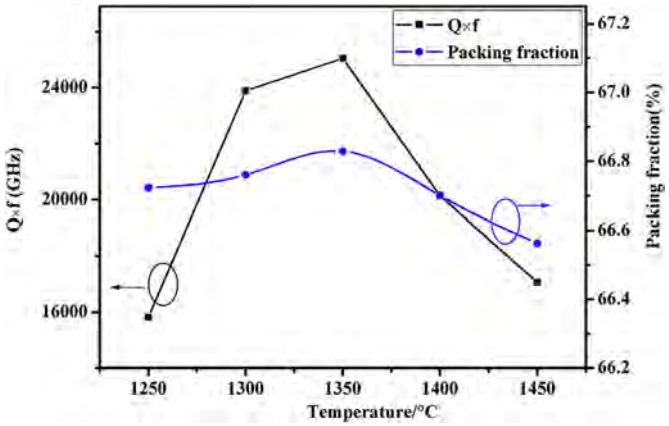

Fig. 10. Relationship between $Q \times f$ values and packing fraction of $NiTiTa_2O_8$ ceramics sintered at various temperatures for 4 h.

Table 3
Interatomic distances (Å) for $NiTiTa_2O_8$ ceramics sintered at different temperatures.

Bond type	St (°C)				
	1400	1250	1350	1300	1450
$d_{A\text{-}O1} \times 2$(Å)	2.0954(1)	2.0362(3)	1.9378(0)	2.0660(7)	2.0960(3)
$d_{A\text{-}O2} \times 4$(Å)	2.1075(8)	1.9752(8)	1.8818(0)	2.0363(7)	2.1075(2)
$d_{B\text{-}O1} \times 2$(Å)	1.9617(3)	1.9951(5)	2.0675(1)	1.9680(8)	1.9525(3)
$d_{B\text{-}O2} \times 2$(Å)	1.9644(2)	1.9581(8)	2.0082(0)	1.9683(8)	1.9655(1)
$d_{B\text{-}O2} \times 2$(Å)	1.9378(0)	2.0902(9)	2.1089(1)	2.0084(3)	1.9461(8)

from 1350 °C to 1450 °C.

The temperature coefficient of the resonance frequency (τ_f) represented the temperature stability of microwave dielectric ceramics. In general, τ_f value of ceramics was associated with the material composition and crystal structure including the ordering degree of cations and the degree of octahedron distortion [31]. Among those factors, the degree of octahedral distortion was corelated with the unsynchronized changes in the length of the chemical bond, which may reflect the restoring force of the tilt recovery and affect the τ_f value. According to the interatomic distances of $NiTiTa_2O_8$ ceramics obtained by Rietveld refinement in Table 3, the octahedral distortions of [AO_6] and [BO_6] were calculated by the equation as follows [13,32]:

$$\Delta[AO_6] = \frac{1}{6}\sum\{(d_i - d_{ave})/d_{ave}\}^2$$

$$\Delta[BO_6] = \left(d_{largest} - d_{smallest}\right)\Big/ d_{ave}$$

where d_i and d_{ave} were an individual and the average bond length of oxygen octahedron. The τ_f values and the distortion of the oxygen octahedral of $NiTiTa_2O_8$ ceramics sintered at different temperature are illustrated in Fig. 11. Overall, the τ_f values of ceramics samples fluctuated between 85 ppm/°C and 67 ppm/°C and presented a slight downward trend with the increase of sintering temperature. The distortions of [AO_6] and [BO_6] octahedra shared the analogous trend which was contrary to that of τ_f values. For microwave dielectric ceramics with rutile structure, E. S. Kim et al. pointed out that the larger oxygen octahedral distortion, the better temperature stability [32,33]. Here, this conclusion was also applicable to $NiTiTa_2O_8$ ceramics on the basis of results shown in Fig. 11. Meanwhile, it also indicated that variations of the chemical bond length and structural evolution had an important impact on the properties. Compared with $NiTiNb_2O_8$ ceramics whose τ_f value was

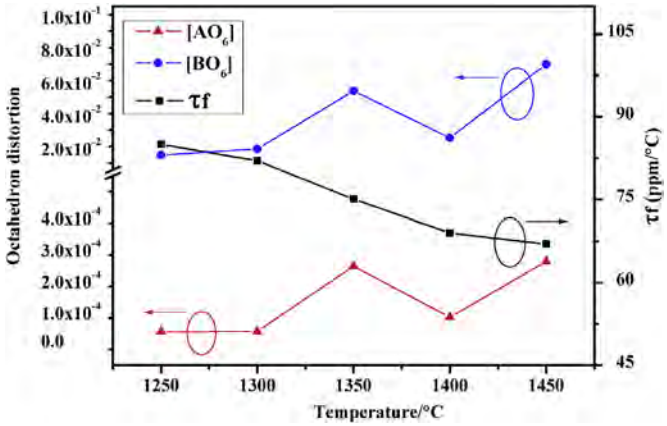

Fig. 11. The τ_f values and the distortion of the oxygen octahedral of $NiTiTa_2O_8$ Ceramics sintered at different temperature.

111.15 ppm/°C [9], the temperature stability of $NiTiTa_2O_8$ ceramics was much better.

4. Conclusions

A new microwave dielectric ceramic $NiTiTa_2O_8$ were synthesized via traditional solid reaction method. The crystal structure, sintering behavior, microstructure and microwave dielectric properties of $NiTiTa_2O_8$ ceramics were studied in this work. Belonging to the tetragonal cell of the trirutile-type structure, the ceramics sintered at 1350 °C possessed the most stable structure with relative density of 94.10% and the overall microstructure depicted irregular polygonal grains. In the range of 1250 °C–1450 °C, the measured dielectric constant which were sensitive to the density of samples varied between 33.81 and 39.86. The $Q \times f$ values were largely associated to relative density and the packing fraction, and the maximum value was obtained at 1350 °C. The variation of τ_f mainly were influenced by the octahedral distortions of [AO_6] and [BO_6]. For $NiTiTa_2O_8$ microwave ceramics sintered at 1350 °C for 4 h, the excellent dielectric properties of $\varepsilon_r = 39.86$, $Q \times f = 25{,}051$ GHz, $\tau_f = 75$ ppm/°C could be obtained.

Acknowledgements

This work has been financially supported by the National Natural Science Foundation of China (No.51772022) and Fundamental Research Funds for the Central Universities (FRF-GF-18-004A)

References

[1] X. S Lyu, L.X. Li, S. Zhang, H. Sun, S. Li, J. Ye, B.W. Zhang, J.T. Li, A new low-loss dielectric material $ZnZrTa_2O_8$ for microwave devices, J. Eur. Ceram. Soc. 36 (2016) 931–935. https://doi.org/10.1016/j.jeurceramsoc.2015.11.015.
[2] A. Baumgarte, R. Blachnik, New $M^{2+}M^{4+}Nb_2O_8$ phases, J. Alloy. Comp. 215 (1994) 117–120, 1994, https://doi.org/10.1016/0925-8388(94)90827-3.
[3] D.W. Kim, D.Y. Kim, K.S. Hong, Phase relations and microwave dielectric properties of $ZnNb_2O_6$–TiO_2, J. Mater. Res. 15 (6) (2000) 1331–1335. https://doi.org/10.1557/JMR.2000.0193.
[4] Y. Zhang, Y. C Zhang, Microwave dielectric properties of sol-gel derived $CoTiNb_2O_8$ ceramics, J. Alloy. Comp. 683 (2016) 86–91. https://doi.org/10.1016/j.jallcom.2016.05.081.
[5] Chin Fang Tseng, Microwave dielectric properties of a new $Cu_{0.5}Ti_{0.5}NbO_4$ ceramics, J. Eur. Ceram. Soc. 35 (2015) 384–387. https://doi.org/10.1016/j.jeurceramsoc.2014.08.027.
[6] Q.J. Mei, C.Y. Li, J.D. Guo, H.T. Wu, Synthesis, characterization, and microwave dielectric properties of ternary-phase ixiolite-structure $MgTiNb_2O_8$ ceramics, Mater. Lett. 145 (2015) 7–10. https://doi.org/10.1016/j.matlet.2015.01.057.
[7] H.L. Pan, L. Cheng, Y.X. Mao, H.T. Wu, Investigation and characterization on crystal structure of ixiolite structure $ATiNb_2O_8$ (A = Mg, Zn) ceramics at microwave frequency based on the complex chemical bond theory, J. Alloy. Comp. 693 (2017) 792–798.
[8] Q.W. Liao, L.X. Lin, X. Ren, X.X. Yu, Q. L Meng, W.S. Xia, A new microwave dielectric material $Ni_{0.5}Ti_{0.5}NbO_4$, Mater. Lett. 89 (2012) 351–353. https://doi.org/10.1016/j.matlet.2012.08.078.
[9] J.X. Bi, C.H. Yang, H.T. Wu, Synthesis, characterization, and microwave dielectric properties of $Ni_{0.5}Ti_{0.5}NbO_4$ ceramics through the aqueous sol–gel process, J. Alloy. Comp. 653 (2015) 1–6. https://doi.org/10.1016/j.jallcom.2015.08.179.
[10] R. Shannon, Revised effective ionic radii and systematic studies of interatomic distances in halides and chalcogenides, Acta Crystallogr. - Sect. A Cryst. Phys. Diffr. Theor. Gen. Crystallogr. 32 (1976) 751–767. https://doi.org/10.1107/S0567739476001551.
[11] Mi Xiao, Yanshuang Wei, Qingqing Gu, Ziqi Zhou, Ping Zhang, Relationships between bond ionicity, lattice energy, bond energy and the microwave dielectric properties of $La(Nb_{1-x}Ta_x)O_4$ (x = 0 - 0.10) ceramics, J. Alloy. Comp. 775 (2019) 168–174. https://doi.org/10.1016/j.jallcom.2018.09.304.
[12] Xin Huang, Huaiwu Zhang, Yuanming Lai, Gang Wang, Mingming Li, Caiyun Hong, Jie Li, Relationship of crystal structure and microwave dielectric properties in $Ni_{0.5}Ti_{0.5}NbO_4$ ceramics with Ta substitution, Eur. J. Inorg. Chem. (2018) 1800–1804. https://doi.org/10.1002/ejic.201800016.
[13] Q. Liao, L. Li, X. Ren, et al., New low-loss microwave dielectric material $ZnTiNbTaO_8$[J], J. Am. Ceram. Soc. 94 (10) (2011) 3237–3240.
[14] Jeong-Hyun Park, Young-Jin Choi, Sahn Nahm, Jae-Gwan Park, Crystal structure and microwave dielectric properties of $ZnTi(Nb_{1-x}Ta_x)_2O_8$ ceramics, J. Alloy. Comp. 509 (2011) 6908–6912. https://doi.org/10.1016/j.jallcom.2011.

03.178.
[15] N. Kumada, Narumi Koike, Kousuke Nakanome, Sayaka Yanagida, Takahiro Takei, Akira Miura, Eisuke Magome, Chikako Moriyoshi & Yoshihiro Kuroiwa. Synthesis of rutile-type solid solution $Ni_{1-x}Co_xTi(Nb_{1-y}Ta_y)_2O_8$ ($0 \leq x \leq 1$, $0 \leq y \leq 1$) and its optical property, J. Asian Ceram. Soc. 5 (2017) 284–289. https://doi.org/10.1016/j.jascer.2017.05.005.
[16] Hongyu Yang, Shuren Zhang, Yawei Chen, Hongcheng Yang, Ying Yuan, Enzhu Li, Crystal chemistry, Raman spectra, and bond characteristics of trirutile-type $Co_{0.5}Ti_{0.5}TaO_4$ microwave dielectric ceramics, Inorg. Chem. 58 (2019) 968–976.
[17] B.H. Toby, EXPGUI, a graphical user interface for GSAS, J. Appl. Crystallogr. 34 (2001), 210e213.
[18] M. Daturi, G. Busca, M.M. Borel, A. Leclaire, P. Piaggio, Vibrational and XRD study of the system CdWO4-CdMoO4, J. Phys. Chem. B 101 (1997) 4358–4369.
[19] B.W. Hakki, P.D. Coleman, A dielectric resonator method of measuring inductive capacities in the millimeter range, Ire Trans. Microw. Theory 8 (1960) 402–410, https://doi.org/10.1109/TMTT.1960.1124749.
[20] W.E. Courtney, Analysis and evaluation of a method of measuring the complex permittivity and permeability microwave insulators, IEEE Trans. Microw. Theory 18 (1970) 476–485, https://doi.org/10.1109/TMTT.1970.1127271.
[21] Y. Kobayashiy, M. Katoh, Microwave measurement of dielectric properties of low-loss materials by the dielectric rod resonator method, IEEE Trans. Microw. Theory 33 (1985) 586–592, https://doi.org/10.1109/TMTT.1985.1133033.
[22] L. Glasser, H.D.B. Jenkins, Lattice energy and unit cell volumes of complex ionic solids, J. Am. Chem. Soc. 122 (2000) 632–638.
[23] H. Lee, I. Kim, K.S. Hong, Dielectric properties of AB_2O_6 compounds at microwave frequencies (A=Ca, Mg, Mn, Co, Ni, Zn, and B=Nb, Ta), J. Appl. Phys. 36 (1997) L1318–L1320 (Part 2, No. 10A).
[24] Y.R. Luo, Comprehensive Handbook of Chemical Bond Energies, CRC Press, 2007.
[25] Y. Zhang, Y.C. Zhang, X.L. Su, M.Q. Xiang, Preparation and characterization of $Bi_2Ti_2O_7$ microwave dielectric ceramics by citrate sol-gel method, Key Eng. Mater. 697 (2016) 219–222. https://doi.org/10.4028/www.scientific.net/KEM.697.219.
[26] R.D. Shannon, Dielectric polarizabilities of ions in oxides and fluorides, J. Appl. Phys. 73 (1993) 348–366. https://doi.org/10.1063/1.353856.
[27] R.D. Shannon, R.A. Oswald, J.B. Parise, B.H.T. Chai, P. Byszewski, A. Pajaczowska, R. Sobolewski, Dielectric constants and crystal structures of $CaYAlO_4$, $CaNdAlO_4$, and $SrLaAlO_4$, and deviations from the oxide additivity rule, J. Solid State Chem. 98 (1992) 90–98. https://doi.org/10.1016/0022-4596(92)90073-5.
[28] R.D. Shannon, Dielectric polarizabilities of ions in oxides and fluorides, J. Appl. Phys. 73 (1993) 348e366.
[29] K. Akinori, O. Hirotaka, O. Hitoshi, Influence of microstructure on microwave dielectric properties of $ZnTa_2O_6$ ceramics with low dielectric loss, J. Alloy. Comp. 337 (2002) 303–308. https://doi.org/10.1016/S0925-8388(01)01950-8.
[30] E.S. Kim, B.S. Chun, R. Freer, R.J. Cernik, Effects of packing fraction and bond valence on microwave dielectric properties of $A^{2+}B^{6+}O_4$ (A^{2+}: Ca, Pb, Ba; B^{6+}: Mo, W) ceramics, J. Eur. Ceram. Soc. 30 (2010) 1731–1736. https://doi.org/10.1016/j.jeurceramsoc.2009.12.018.
[31] M. Wu, Y. Zhang, J. Chen, M. Xiang, Microwave dielectric properties of sol-gel derived $NiZrNb_2O_8$ ceramics, J. Alloy. Comp. 747 (2018) 394–400. https://doi.org/10.1016/j.jallcom.2018.02.300.
[32] E.S. Kim, D.H. Kang, Relationships between crystal structure and microwave dielectric properties of $(Zn_{1/3}B^{5+}_{2/3})_xTi_{1-x}O_2$($B^{5+}$=Nb, Ta) ceramics, Ceram. Int. 34 (2008) 883–888.
[33] D.H. Kang, E.S. Kim, Microwave dielectric properties of rutile $(Zn^{1/3}Nb^{2/3})_{0.40}(Ti_{1-x}Sn_x)_{0.60}O_2$ ($0.15 \leq x \leq 0.30$), ceramics, Ceram. Int. 34 (4) (2008) 889–892.